Magnetospheric electron density long-term (>1 day) refilling rates inferred from passive radio emissions measured by IMAGE RPI during geomagnetically quiet times

R. E. Denton,[1] Y. Wang,[2,3] P. A. Webb,[3] P. M. Tengdin,[1] J. Goldstein,[4] J. A. Redfern,[4] and B. W. Reinisch[5]

Received 19 October 2011; revised 28 December 2011; accepted 27 January 2012; published 17 March 2012.

[1] Using measurements of the electron density n_e found from passive radio wave observations by the IMAGE spacecraft RPI instrument on consecutive passes through the magnetosphere, we calculate the long-term (>1 day) refilling rate of equatorial electron density $dn_{e,eq}/dt$ from $L = 2$ to 9. Our events did not exhibit saturation, probably because our data set did not include a deep solar minimum and because saturation is an unusual occurrence, especially outside of solar minimum. The median rate in cm^{-3}/day can be modeled with $\log_{10}(dn_{e,eq}/dt) = 2.22 - 0.006L - 0.0347L^2$, while the third quartile rate can be modeled with $\log_{10}(dn_{e,eq}/dt) = 3.39 - 0.353L$, and the mean rate can be modeled as $\log_{10}(dn_{e,eq}/dt) = 2.74 - 0.269L$. These statistical values are found from the ensemble of all observed rates at each L value, including negative rates (decreases in density due to azimuthal structure or radial motion or for other reasons), in order to characterize the typical behavior. The first quartile rates are usually negative for $L < 4.7$ and close to zero for larger L values. Our rates are roughly consistent with previous observations of ion refilling at geostationary orbit. Most previous studies of refilling found larger refilling rates, but many of these examined a single event which may have exhibited unusually rapid refilling. Comparing refilling rates at solar maximum to those at solar minimum, we found that the refilling rate is larger at solar maximum for small $L < 4$, about the same at solar maximum and solar minimum for $L = 4.2$ to 5.8, and is larger at solar minimum for large $L > 5.8$ such as at geostationary orbit ($L \sim 6.8$) (at least to L of about 8). These results agree with previous results for ion refilling at geostationary orbit, may agree with previous results at lower L, and are consistent with some trends for ionospheric density.

Citation: Denton, R. E., Y. Wang, P. A. Webb, P. M. Tengdin, J. Goldstein, J. A. Redfern, and B. W. Reinisch (2012), Magnetospheric electron density long-term (>1 day) refilling rates inferred from passive radio emissions measured by IMAGE RPI during geomagnetically quiet times, *J. Geophys. Res.*, *117*, A03221, doi:10.1029/2011JA017274.

1. Introduction

[2] The overall convection of plasma across the equatorial magnetosphere is controlled by a competition between sunward flow (magnetospheric convection) and corotation that drags flux tubes around the Earth [*Grebowsky*, 1970; *Goldstein and Sandel*, 2005]. During geomagnetic storms, during which magnetospheric convection becomes stronger, plasma that had been rotating around the Earth may be swept away to the magnetopause where it is entrained in the magnetosheath flow [e.g., *Goldstein et al.*, 2003; *Chen and Moore*, 2006] and a new boundary between high density close to the Earth (the plasmasphere) and low density farther from the Earth (the plasmatrough) may form [*Grebowsky*, 1970; *Goldstein and Sandel*, 2005]. Then if geomagnetic condition becomes more quiet, these low density regions may start to corotate with the Earth [*Grebowsky*, 1970; *Goldstein and Sandel*, 2005]. As the flux tubes rotate, refilling of these flux tubes occurs [*Singh and Horwitz*, 1992; *Lemaire and Gringauz*, 1998].

[3] Refilling is usually thought to be dominated by upward flow of particles from the ionosphere, though other processes may occur, such as non-corotation convection and perhaps interchange at large distances from the Earth [*Lemaire and Gringauz*, 1998; *Darrouzet et al.*, 2008]. The exact process and populations involved in upward flow from the ionosphere may be complicated, but quiet time refilling usually leads to an increase in low energy (~1 eV) particles.

[1]Department of Physics and Astronomy, Dartmouth College, Hanover, New Hampshire, USA.
[2]NASA Goddard Space Flight Center, Greenbelt, Maryland, USA.
[3]Goddard Earth Sciences and Technology Center, University of Maryland, Baltimore County, Baltimore, Maryland, USA.
[4]Southwest Research Institute, San Antonio, Texas, USA.
[5]Center for Atmospheric Research, University of Massachusetts at Lowell, Lowell, Massachusetts, USA.

0148-0227/12/2011JA017274

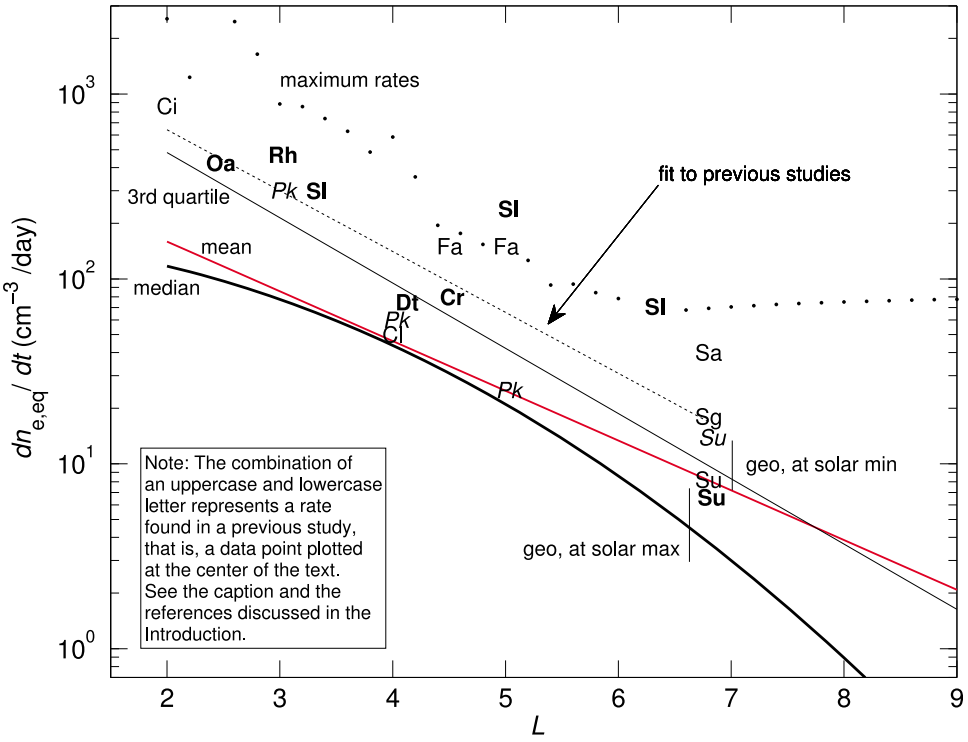

Figure 1. Base 10 logarithm of the equatorial electron density long-term (>1 day) refilling rate dn_e/dt in cm^{-3}/day versus L inferred from various studies described in the Introduction; the symbol for each rate is composed of the first and last letter of the first author of each reference. Rates determined during solar maximum are in boldface, while rates determined at solar minimum are in italics. The black dotted line is a linear fit using all the rates referenced, while the black thick solid curve, the black thin solid line, and the red solid line are the median, third quartile, and mean values found in this study. The short vertical lines labeled "geo, at solar max" and "geo, at solar min" extend from the median to third quartile values of dn_e/dt found in our study at geostationary orbit (L = 6.8) for solar maximum (2001 and 2002) and solar minimum (late 2003 to 2006), respectively; these are offset horizontally from their real position which is horizontally roughly in the center of the "Su" symbols. The dots are the maximum rates found in our study.

Superimposed on the long-term >1 day refilling is a daily pattern of upflow on the dayside and downflow on the nightside [*Singh and Horwitz*, 1992; *Lemaire and Gringauz*, 1998]. But here we are interested in the long-term refilling rate.

[4] In addition to refilling in the plasmatrough, there is also evidence that refilling occurs in the (large L) outer part of the plasmasphere [*Park*, 1974; *Reinisch et al.*, 2004]. Some studies indicate that refilling will slow when a saturated (or asymptotic) density is reached [*Park*, 1974; *Song et al.*, 1988; *Lawrence et al.*, 1999; *Su et al.*, 2001]. (Note that the "saturated density" of *Carpenter and Anderson* [1992] is an average of plasmasphere densities observed after periods of relatively steady or quiet conditions for at least 62 hours, not a theoretical upper limit.)

[5] *Park* [1974] used whistler wave data [*Helliwell*, 1965] to infer values of refilling rate for electron density n_e field line integrated flux tube content (in cm^{-2}/day) for one event within the outer plasmasphere during June 1965 (solar minimum). Using a diffusive equilibrium field line distribution (which is not a bad assumption in the plasmasphere [*Denton et al.*, 2004]), *Park* [1974, Figure 3] plotted equatorial electron density values. Roughly from this plot, we find that n_e increases by 300 cm^{-3}/day at L = 3, by 60 cm^{-3}/day at L = 4, and by 25 cm^{-3}/day at L = 5. We plot these refilling rates in Figure 1 using the symbol "Pk" composed of the first and last letter of the first author's name. Similarly, rates for references mentioned below (except for the work of *Lawrence et al.* [1999], which we take to be superceded by the work of *Su et al.* [2001]) are plotted in the same way. (Su et al. used the same method as Lawrence et al. but with a larger data set.) Bold, normal face, and italics correspond to observations at solar maximum, rising or falling phase of the solar cycle, and solar minimum, respectively. Since the rates observed by Park were measured at solar minimum, we use italics for the "Pk" symbol in Figure 1.

[6] *Chappell* [1974] states that the refilling rate for n_e can reach 50 cm^{-3}/day based on measurements by the OGO 5 spacecraft at L = 4. *Carpenter et al.* [1993], using measurement of ion density from the DE-1 spacecraft, found an n_e refilling rate of 80 cm^{-3}/day at L = 4.5 for an event observed during the summer of 1982 (solar maximum). Using ion composition measurements on the GEOS 1 spacecraft, *Farrugia et al.* [1989] found for three events during 1977 and 1978 (solar minimum to rising phase of solar cycle) an n_e refilling rate of 150 cm^{-3}/day at L = 4.5

and 5. *Reinisch et al.* [2004] used data from active radio sounding by the Imager for Magnetopause-to-Aurora Global Exploration (IMAGE) spacecraft Radio Plasma Imager (RPI) instrument to study refilling of n_e; based on data in their paper, we infer a refilling rate of at least 470 cm^{-3}/day at $L = 3$ for one event in April 2000 (solar maximum).

[7] A large amount of research on refilling has been done at geostationary orbit ($L \sim 6.6$). *Sojka and Wrenn* [1985] used particle measurements by the GEOS-2 spacecraft for five events from 1978 to 1980 (rising phase of solar cycle) to find typical refilling rates between 30 and 50 cm^{-3}/day. Based on 11 refilling events using plasma wave measurements by GEOS-2, *Song et al.* [1988] found that the refilling rate (at dusk MLT) was typically 25 cm^{-3}/day if the minimum Dst during the past 24 hours was 0 nT, but that the refilling rate was typically 10 cm^{-3}/day if the minimum Dst during the last 24 hours was −50 nT. They found that the saturation density was about 70 cm^{-3}. *Lawrence et al.* [1999] used the LANL spacecraft MPA ion particle instrument from 1990 to 1997 (solar maximum to solar minimum) to find two stages of refilling with an early time (0.5 to 1 days) refilling rate of 0.6 to 12 cm^{-3}/day, and a later refilling rate of 10–50 cm^{-3}/day to saturation of about 50–100 cm^{-3}. *Su et al.* [2001] used a larger set of data from 1990 to nearly 2001 (11 years over an entire solar cycle) to find similar but somewhat different rates, between 2.5 to 6.5 cm^{-3}/day for early time refilling (0.5 to 1 days), and between 10 and 25 cm^{-3}/day for late time refilling to a saturation density of 100 to 200 cm^{-3}. Su et al. were able to study the solar cycle dependence with average late time refilling rates of 7.7 cm^{-3}/day at solar maximum, 10.0 cm^{-3}/day at the rising or falling phases of the solar cycle, and 18.6 cm^{-3}/day at solar minimum. Su et al. found that there was no local time dependence to the refilling rate, and that the early time refilling rate increased with geomagnetic activity as indicated by the Kp index. (For the purposes of plotting the refilling rate in Figure 1, we use 0.33 times the early refilling rate plus 0.67 times the late time refilling rate.)

[8] *Chi et al.* [2000] investigated refilling of mass density at $L = 2$ using ground magnetometer data for an event in September 1998 (rising phase of solar cycle). Based on Figure 2 of *Chi et al.* [2000], we estimate that the rate of refilling is 860 amu/cm^3/day. Results to date [*Takahashi et al.*, 2006, 2008; *Dent et al.*, 2006] suggest that the mass density is a good proxy for electron density within the plasmasphere, though there may be a tendency for the average ion mass to be somewhat higher than 1 amu at $L < 3$ [*Dent et al.*, 2006, Figure 8]. Dent et al. studied mass density refilling at $L = 4.1$ for an event in May 2001 (solar max). Their event was in the plasmatrough, for which it is not as clear that the mass density will be such a good proxy for the electron density. They show a range of refilling rate increasing from low values 0–77 amu/cm^3/day at early times to 32–700 amu/cm^3/day at later times. The median value is 75 amu/cm^3/day (and we plotted this in Figure 1). *Obana et al.* [2010] found that the mass density refilling rate for an event at $L \sim 2.45$ in April 2001 (solar maximum) was 424 amu/cm^3/day.

[9] *Sandel and Denton* [2007] used data from the IMAGE Extreme Ultraviolet Imager (EUV) instrument to calculate local time averaged refilling rates of He+ for an event in June 2001 (solar max). While there are assumptions required to infer the local He+ density, this technique is promising because it can in principle get a global picture of refilling. They find a refilling rate for He+ of 24 cm^{-3}/day at $L = 3.3$, 10 cm^{-3}/day at $L = 5$ [from *Sandel and Denton*, 2007, Figure 3] and about 1.7 cm^{-3}/day at $L = 6.3$. Using $n_{He+}/n_{H+} = 0.081$, 0.041, and 0.024 based on the formulas of *Craven et al.* [1997] at F10.7 ∼ 170 (in units of 10^{-22} W m^{-2} Hz^{-1}), we find approximate n_e refilling rates of 300 cm^{-3}/day at $L = 3.3$, 240 cm^{-3}/day at $L = 5$, and about 71 cm^{-3}/day at $L = 6.3$.

[10] We are aware of a number of other studies on refilling [e.g., *Fu et al.*, 2010], but most of these describe short term (less than a day) variation of the density with respect to a magnetic local time MLT that is periodic. Such studies cannot describe long-term quiet time refilling.

[11] First of all, note that most of the references that we have described use a single event. Studies involving a large number of events are at geostationary orbit, those of *Song et al.* [1988] (which unfortunately is not very well described) and *Lawrence et al.* [1999] and *Su et al.* [2001]. One danger for studies using a single event is that the event could be picked based on especially noticeable (that is, large) refilling. This might bias the refilling rates upward.

[12] Secondly, based on previous studies, the solar cycle dependence is not clear. Most studies at solar maximum (boldface in Figure 1) show higher refilling rates than those at solar minimum (italics in Figure 1), but this is opposite to the trend observed by *Su et al.* [2001] (with the most data).

[13] Finally, for reference we fit all the data plotted in Figure 1 (admittedly a questionable procedure), and find the following rate for electron density refilling dn_e/dt in cm^{-3}/day versus L,

$$\frac{dn_e}{dt} = 10^{3.48-0.331L}\left(\mathrm{cm}^{-3}/\mathrm{day}\right). \tag{1}$$

Or we can fit the data with

$$\frac{dn_e}{dt} = 10400L^{-3.25}\left(\mathrm{cm}^{-3}/\mathrm{day}\right). \tag{2}$$

Note that the dependence in (1) is quite similar to the plasmasphere radial dependence for n_e of *Carpenter and Anderson* [1992], which is (neglecting the periodic local time dependence and a small sunspot number dependence that falls off rapidly for $L > 2$)

$$n_{e,CA} = 10^{3.90-0.315L}\left(\mathrm{cm}^{-3}\right). \tag{3}$$

Dividing (3) by (1) yields a characteristic refilling time (time to fill from zero density to Carpenter and Anderson's average plasmasphere density) of

$$\tau_{\mathrm{References}} = 10^{0.016L}(2.63\ \mathrm{days}), \tag{4}$$

that is almost constant, varying from 2.9 days at $L = 3$ to 3.4 days at $L = 6.8$ (a typical L shell for LANL spacecraft at geostationary orbit [*Denton et al.*, 2011]); this is plotted as the dotted curve in Figure 2. Even assuming that this formula is correct, it doesn't necessarily mean that the observed refilling times will always be constant with respect to L because the fractional depletion of n_e after a storm may be different for different L. Note also that the refilling rate of

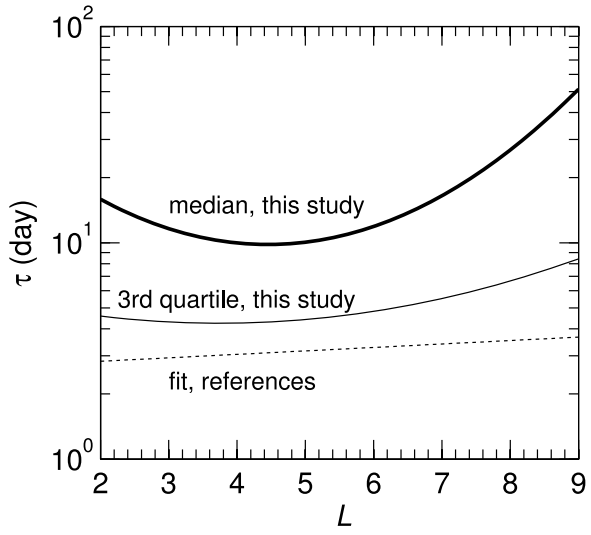

Figure 2. Refilling time defined as the plasmasphere density of *Carpenter and Anderson* [1992] (equation (3)) divided by the refilling rate $dn_{e,eq}/dt$ for the median refilling rate found in our study (thick solid curve), the third quartile refilling rate found in our study (thin solid curve), and the best least squares fit to the references listed in section 1 and shown in Figure 1 (dotted curve).

(1) $\propto L^{-3.25}$ is less but not greatly less steep than the rough L^{-4} dependence expected for flux tube volume varying as L^4 (characteristic flux tube length L times flux tube area $\propto 1/B \sim L^3$). (We did a more accurate integration to show that flux tube volume $\propto L^{4.1}$ for L = 3–8 if the area is constant at the foot point of the field line.)

[14] The purpose of this study is to use a large number of refilling events observed by IMAGE RPI in the passive data mode (observing natural radio emissions [*Reinisch et al.*, 2001]) in order to derive statistically significant refilling rates over a large range of L shell. We will not limit the data to positive refilling rates, and will determine the first quartile, median (second quartile), third quartile, and mean refilling rates in order to characterize the distribution of rates. Note that we are calculating the refilling rate using the observed rate of change of density, so what we are calling refilling could include more physical effects than just upward flow of plasma from the ionosphere. Presumably these other effects are reduced relative to more active times for the geomagnetically quiet times that we consider. Negative rates can result from azimuthal structure (because we don't see the same flux tube at the next satellite pass), radial motion, or for other reasons.

[15] Our technique calculates the refilling rate based on spacecraft traversals through the same region of MLT separated in time by roughly 14 hours (the period of IMAGE's orbit). It should be understood at the outset that we are not measuring an increase in density of a single flux tube. In fact there is no technique, including the use of data on the ground or at geostationary orbit, that can do so (flux tubes may move radially and do not exactly co-rotate). But our hope is that by using a large number of events and looking at statistical quantities such as quartile values, we can roughly characterize the typical "global refilling" (independent of MLT) which occurs.

2. Data and Details Concerning Method

[16] A database of electron density measurements has been prepared from passive radio emissions observed by IMAGE RPI [*Webb et al.*, 2007]. Only data in the Level Zero Telemetry L0 format were used (details about the RPI data can be found at http:ulcar.uml.edu/rpi.html). This limited the dates of density measurements to roughly between the beginning of 2001 to the end of 2005. An automatic plasma frequency detection algorithm was used to match emission peaks to upper hybrid or Z-mode emission using the T96 magnetic field model [*Tsyganenko*, 1996] for the electron gyrofrequency and using an algorithm motivated by results of *Benson et al.* [2004]. (*Benson et al.* [2004] showed that an upper hybrid or Z-mode peak extends from the electron gyrofrequency to the upper hybrid frequency.) If that was not successful, the algorithm searched for a plasma frequency continuum edge [*Persoon et al.*, 1983]. While most data points could be detected using the automatic procedure, some manual correction was necessary. The end result was a database of about 205,000 n_e measurements.

[17] The IMAGE orbit was polar with a period of about 14 hours. We divide these orbits into half orbits from perigee to apogee, or from apogee to perigee. During a period of several days, IMAGE sampled roughly two distinct MLT values on opposite sides of the Earth every 14 hours. From the passive radio data, we then determined a profile of n_e versus L, where L means the farthest radial extent in units of Earth radii R_E of any point on a field line connecting to the position of IMAGE using the TS05 magnetic field model *Tsyganenko and Sitnov* [2005]. Only data points for which the radius of farthest extent was within 5% of the radius of minimum magnetic field (from the TS05 model) were used in order to eliminate cusp field lines for which the field line dependence is not known.

[18] Because the IMAGE spacecraft has a polar orbit, and the magnetic latitude MLAT is not always near zero, we need to adjust the n_e values to an equatorial value before calculating refilling rates. *Denton et al.* [2002] assumed a power law form for the density variation along field lines,

$$n_e = n_{e,eq}\left(\frac{LR_E}{R}\right)^{\alpha}, \tag{5}$$

where $n_{e,eq}$ is the equatorial electron density, and modeled α with

$$\alpha = 8 - 0.43L - 3\log_{10}(n_{e,eq}) + 0.28(\log_{10}(n_{e,eq}))^2. \tag{6}$$

[19] But when *Denton et al.* [2006] examined field line distributions of density from active RPI sounding (probably the best technique for determining the field line dependence when active sounding traces are available; see references in their paper), they found that the α values predicted by (6) were too low in the plasmasphere (typically by about 0.5). Because of this, we use a model for α similar to (6), but with the addition of an extra term 0.5 $\log_{10}(n_{e,eq}/(n_{e,CA}/10))$. Our intention is to increase α in the plasmasphere, where $n_{e,eq} \sim$

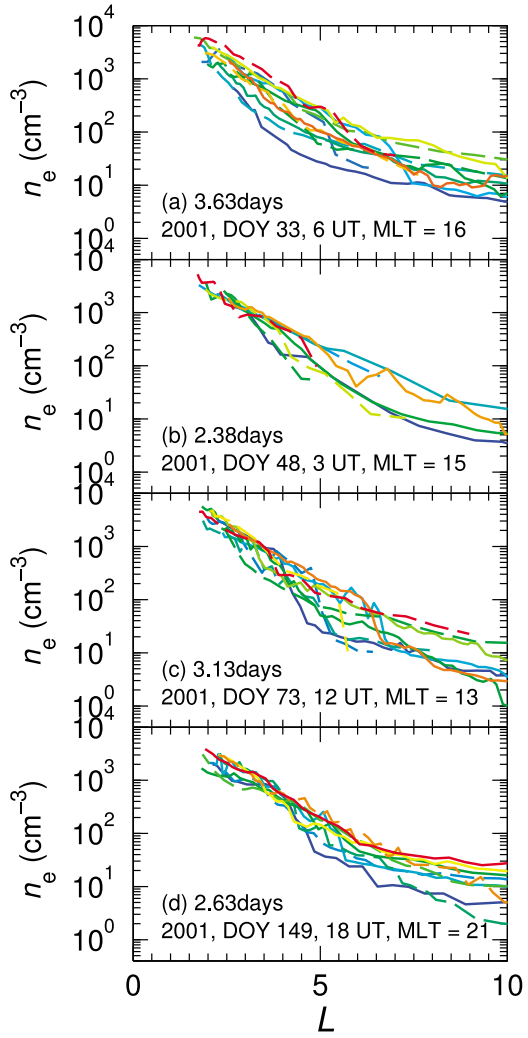

Figure 3. Electron density n_e profiles versus L for the first four quiet time intervals with Kp < 1.5 for at least 2.05 days. (a–d) Each panel lists the number of days of the total interval and the starting time and approximate MLT value for the first profile. The time of the profiles is indicated by the color, with dark blue corresponding to the first time, and dark red corresponding to the last time for times separated by approximately 7 hours. The solid curves are approximately for the MLT listed, while the dashed curves are on the opposite side of the Earth (MLT value listed ± 12).

$n_{e,CA}$, but not in the plasmatrough, where $n_{e,eq} \sim n_{e,CA}/10$. Plugging in $n_{e,CA}$ from (3) into (6), we get

$$\alpha = 6.55 - 0.27L - 2.5\log_{10}(n_{e,eq}) + 0.28(\log_{10}(n_{e,eq}))^2. \quad (7)$$

One nice feature of this adjustment, considering that we would like to avoid extreme values, is that the L and $n_{e,eq}$ dependencies are weaker than in the original model. We make a further limitation that we do not allow *alpha* values outside of the range 0.5–3.5. We expect theoretically a range of α between 0 for diffusive equilibrium (which may develop after a long period of quiet) and 4 for exospheric equilibrium (which should develop after several hours; see *Lemaire and Gringauz* [1998, section 5.2.5] and discussion by *Denton* [2006]). Results by *Denton et al.* [2006] suggest that α is usually greater than or equal to 0.5; we conservatively chose an upper limit of 3.5 (0.5 less than the typical upper limit like we used 0.5 greater than the typical lower limit). At any rate, we implement these limits as follows: if our formula predicts a value of α outside of the limit, we adjust it to the limiting value.

[20] In order to use (7), we need to know the equatorial electron density, but we measure n_e at an off-equatorial site. In order to self consistently evaluate $n_{e,eq}$ and α, we use an iterative procedure whereby we first use the measured n_e in $n_{e,eq}$, then evaluate $n_{e,eq}$ using (5), then evaluate a new α using $n_{e,eq}$ in (7), and so on. Using the limitation of α to values within 0.5–3.5, the iteration always converges. (It does not always converge if we do not impose this limitation.)

3. Results

3.1. Quiet Time Events With Kp < 1.5

[21] We first set out to find time periods of low geomagnetic activity, for which it is expected that refilling may occur out to a large distance. Similar to *Lawrence et al.* [1999] and *Su et al.* [2001], we first chose time periods with hourly average (interpolated from 3 hour values) of the Kp index less than 1.5. Then we looked for time periods of at least 2.05 days. (This apparently arbitrary difference from 2.0 days was used to ensure that we could plot all the events in one figure using our current format.) There were 37 periods between 2001 and the end of 2005 meeting this criterion. Of these, there were 34 time periods with at least two profiles of n_e. Of these, 30 time periods had at least two profiles of n_e at roughly two opposing MLT values (one on either side of the Earth). So in terms of time periods, there are 34 events, but in terms of independent MLT profiles, there are 64 events.

[22] Figure 3 shows profiles of n_e versus L for the first four of these events. These density values are the measured n_e values, not the $n_{e,eq}$ values using (5) with (7). In each panel, profiles at early times have more bluish hues, while profiles at late times have more reddish hues so that one can see the development in time. (The order is that of the rainbow, blue to cyan to green to yellow to orange to red.) The solid curves are at the MLT value listed in the panel, while the dashed curves are at the opposing MLT value (MLT ± 12). Generally, densities at early times (more bluish hue) are lower while densities at later times (more reddish hue) are higher, but this is not always the case. For instance, in Figure 3b, the solid cyan curve is above the solid blue curve as expected, but it is also above the solid orange curve which is not expected. Because of this, the linear refilling rate will usually be positive, but there may be events for which the refilling rate is negative (at least at a certain L).

[23] Figure 4 shows $n_{e,eq}$ values at $L = 6.8$ versus time in days from the start of the quiet time interval for each of the 34 quiet time events. Each data point is found by linearly interpolating $\log_{10}(n_e)$ values from the curves like the ones plotted in Figure 3 to $L = 6.8$ and then adjusting for the field line dependence using (5) with (7) with the limitation $0.5 \leq \alpha \leq 3.5$. At the upper left of each panel, the event number is shown followed by the date (with fractional day of year DOY) and the MLT value of the first measurement and that

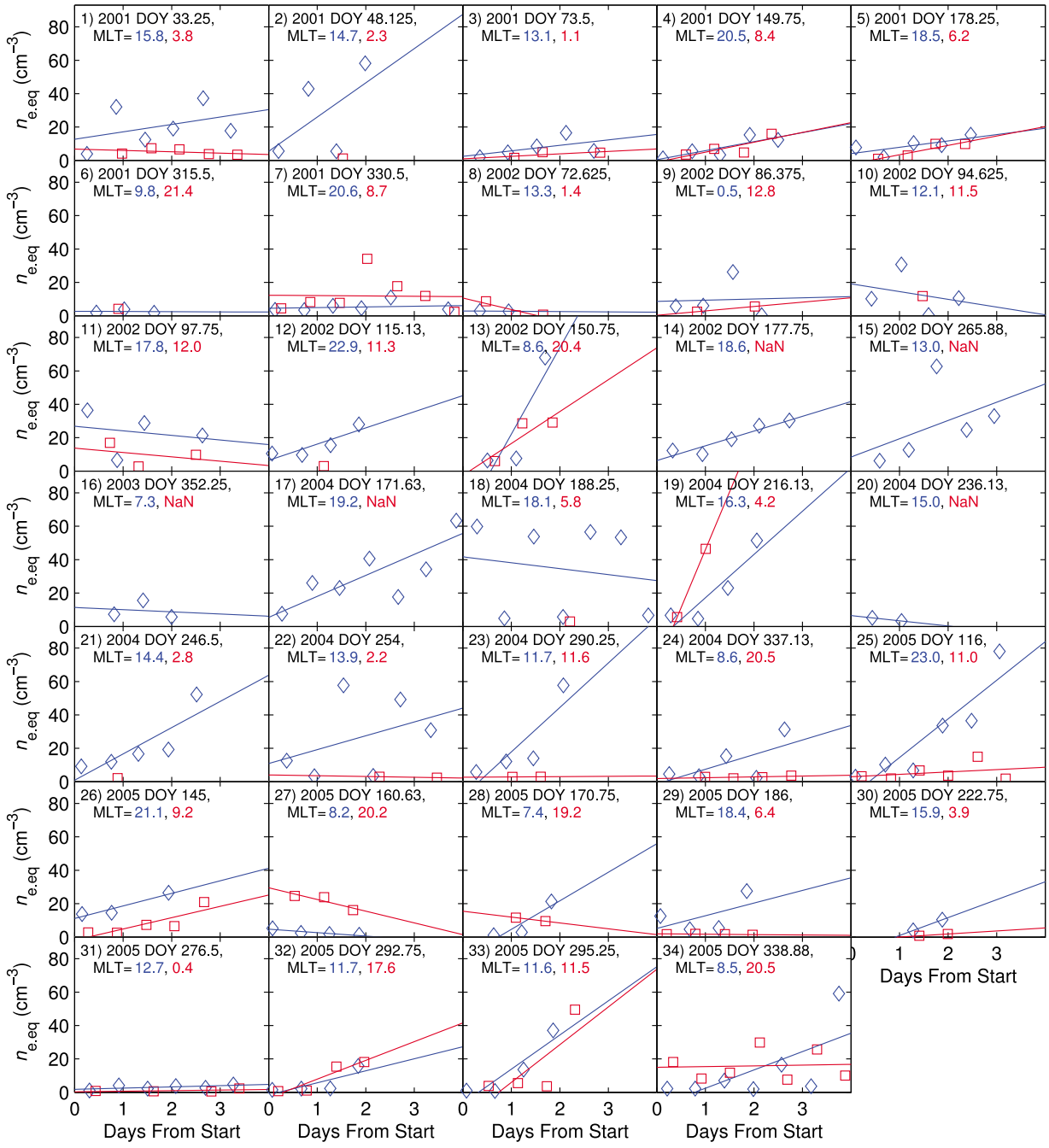

Figure 4. Equatorial electron density $n_{e,eq}$ measured at $L = 6.8$ versus day from the start of the quiet time interval for all 34 quiet time intervals with Kp < 1.5 for at least 2.05 days. The blue diamonds are the measurements at the MLT value of the first measurement within the interval, while the red squares are at the opposing (±12) MLT value. In each panel, the event number is listed, followed by the starting date of the quiet time interval (with fractional day of year DOY), and then the MLT values (in fractional hours) for the MLT of the first measurement (MLT of measurements plotted as blue diamonds) and the opposing MLT value (MLT of measurements plotted as red squares).

of the measurements on the opposite side of the Earth. The blue diamonds show $n_{e,eq}$ values at approximately the first MLT value listed, while the red squares show $n_{e,eq}$ values at approximately the second MLT value listed ("NaN" = "not a number" indicates that there are no measurements at the opposite side of the Earth). The blue and red lines are the best linear least squares fit to the data points with the same color.

[24] The linear refilling rate $dn_{e,eq}/dt$ is the slope of each blue or red line in each panel of Figure 4, and since the horizontal and vertical scales are the same in each panel, the slopes can be easily compared. We note several things about the data in this figure. The first characteristic that stands out

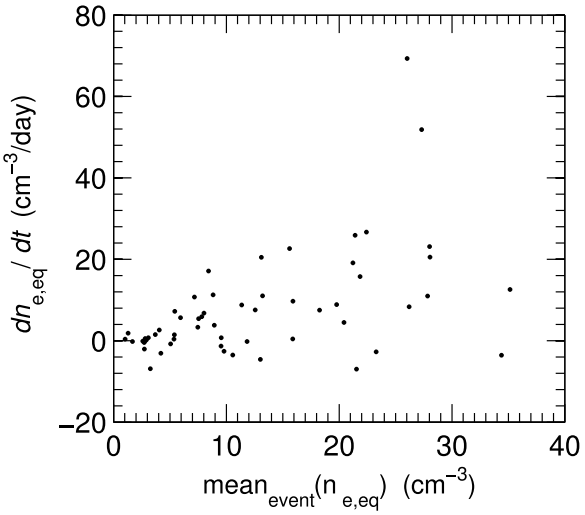

Figure 5. Linear refilling rate $dn_{e,eq}/dt$ versus the mean equatorial electron density for each event mean$_{event}$($n_{e,eq}$) at $L = 6.8$.

very clearly is that there is a very large range of possible linear refilling rates depending on which event is chosen. And this suggests that the same thing would be true for any refilling study such as ours that uses measurements from a spacecraft that periodically returns to a certain MLT value.

[25] Secondly, it's possible that there is a slight tendency for the refilling rate to be lower during the first day (as suggested by *Lawrence et al.* [1999], *Su et al.* [2001], and *Dent et al.* [2006]), but this distinction is not very clear. There are 57 lines corresponding to two or more red or blue data points in Figure 4. Of these, we judge that 15 could be considered to show evidence of a lower refilling rate during the first day, for instance the blue data points in event 19 or 28. On the other hand, 8 of the data points could be considered to show the opposite trend, for instance the blue data points for events 2 or 10. Most of the events do not present evidence of any bias toward lower or higher refilling rate during the first day.

[26] Third, there does seem to be a population of events for which the density and refilling rate are low. Figure 5 shows the linear refilling rate $dn_{e,eq}/dt$ versus the mean equatorial electron density mean$_{event}$($n_{e,eq}$) for each event at $L = 6.8$. There is a slightly (though not greatly) higher density of data points with low mean$_{event}$($n_{e,eq}$). Seeing as the mean density is low, it's not surprising that these data points have a small refilling rate. (If the value is always small, it could not have ever increased steeply.) For the higher mean densities, the refilling rates seem to be evenly distributed to about twice the mean density (like $dn_{e,eq}/dt$ in cm^{-3}/day = 2 mean$_{event}$($n_{e,eq}$) in cm^{-3}), which means that the refilling time is 0.5 day for a change in density equal to the mean density, or about 1 day for a change in density equal to two times the mean density (∼maximum density).

[27] Finally, in this data set we don't see a clear trend for saturation at a high value. We will discuss this further below. But generally we find it sufficient to characterize each set of blue or red data points in Figure 4 with a single linear refilling rate. Figure 6 shows data in the same format as Figure 4, but for $L = 3$. The same observations that we made about Figure 4 also apply to Figure 6.

[28] While Figures 4 and 6 indicate that there is an extremely large variation in refilling rate, we can characterize the distribution in refilling rate by finding the quartile and mean values of the individual refilling rates (slope of the lines plotted in Figures 4 and 6). Azimuthal structure will lead to outliers. For instance, if the spacecraft is initially in the plasmatrough, and later is in the plasmasphere due to azimuthal structure, the refilling rate may appear unusually large. And if the spacecraft is initially in the plasmasphere, and later is in the plasmatrough, the refilling rate may be unusually low or even negative. We expect, however, that the median refilling rate will give a useful measure of what typically occurs. Figure 7b shows a histogram of our refilling rates for the events observed at $L = 6.8$ along with vertical lines that indicate the first quartile, median, and third quartile values.

[29] Our method depends on the assumption that there is no significant dependence of the refilling rate on MLT. This is shown in Figure 8, where individual refilling rates $dn_{e,eq}/dt$ (slopes of the blue or red lines in figures such as Figures 4 and 6) are plotted versus MLT after normalization to the median refilling rate at each particular L value median$_L$($dn_{e,eq}/dt$). Data points are plotted for a range of L values between 2 and 9 (0.5 increment). The top panel shows a linear scale while the bottom panel shows positive values on a log scale. The plotted ranges show most, but not all of the data. Because of the normalization, the median value for all the data points at each L shell is unity. Clearly there is no significant dependence on MLT.

3.2. Long-Term Refilling Rates

[30] Now we calculate the refilling rates at L values between 2 and 9 and show the first quartile, median (2nd quartile), 3rd quartile, and mean values in Figure 9. Figure 9a plots $dn_{e,eq}/dt$ versus L on a linear scale, whereas Figure 9b plots $dn_{e,eq}/dt$ versus L on a log scale.

[31] The first quartile values (lower thin solid black curves in Figures 9a and 9b) are most often negative, which accounts for the absence of this curve (missing data points) for most L values in Figure 9b. A rough fit (minimizing the least squares error) to the first quartile value of $dn_{e,eq}/dt$ is

$$\frac{dn_{e,eq}}{dt} = -20.\ (4.7 - L)^2 \left(\mathrm{cm}^{-3}/\mathrm{day}\right), \quad \text{for } L < 4.7, \tag{8}$$

and $dn_{e,eq}/dt = 0$ for $L \geq 4.7$. This fit is plotted as the dotted curve in Figure 9a.

[32] A quadratic fit for the median value of the base 10 logarithm of $dn_{e,eq}/dt$ (thick solid black curves in Figures 9a and 9b) yields

$$\frac{dn_{e,eq}}{dt} = 10^{2.22 - 0.006L - 0.0347L^2} \left(\mathrm{cm}^{-3}/\mathrm{day}\right), \tag{9}$$

plotted as the thick dotted curve in Figure 9b.

[33] A linear fit for the third quartile value of the base 10 logarithm of $dn_{e,eq}/dt$ (upper thin solid black curve in Figures 9a and 9b) yields

$$\frac{dn_{e,eq}}{dt} = 10^{3.39 - 0.353L} \left(\mathrm{cm}^{-3}/\mathrm{day}\right), \tag{10}$$

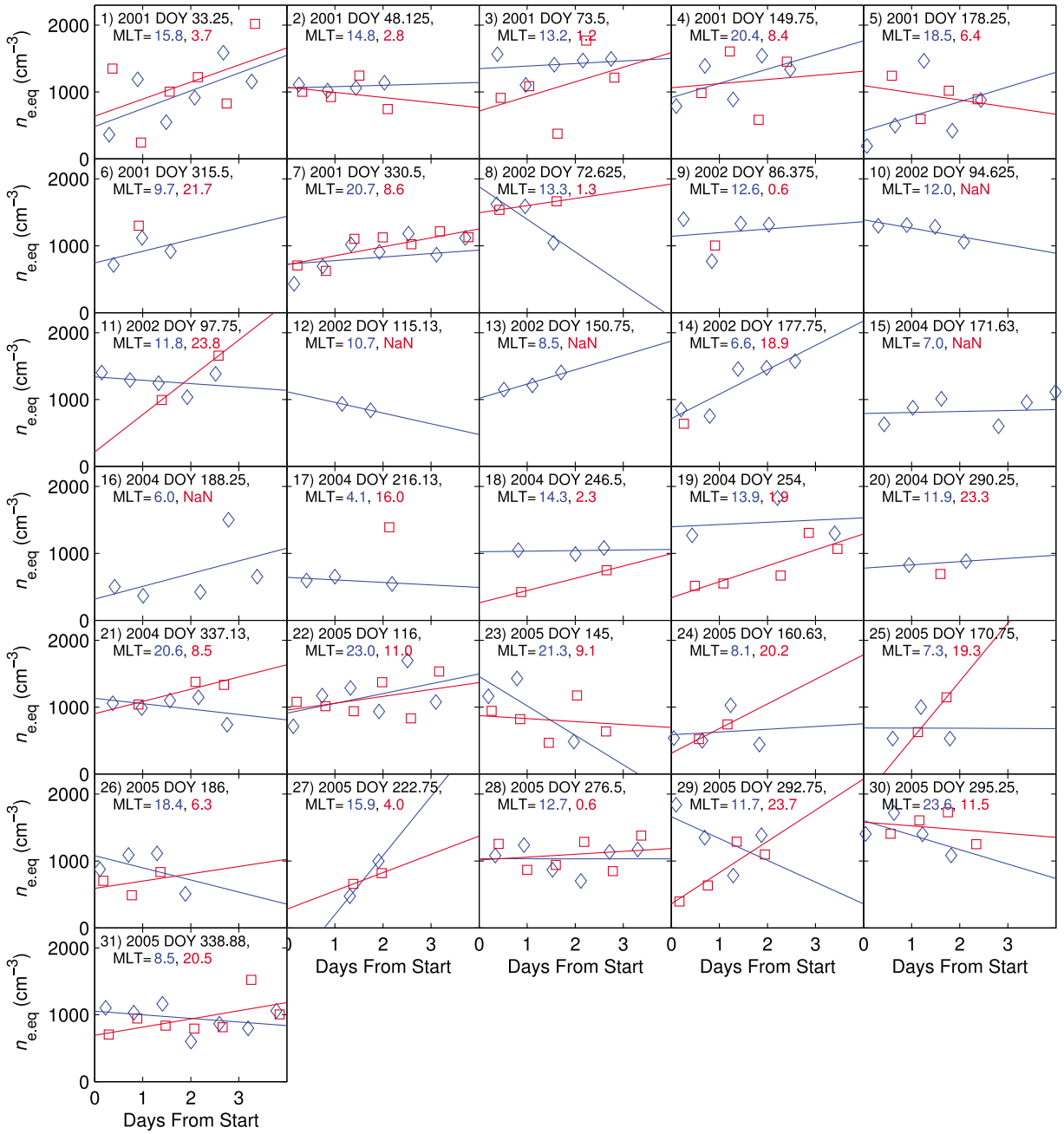

Figure 6. Same as Figure 4 except for n_e measurements at $L = 3$.

and this is plotted as the thin dotted curve in Figure 9b. (Note that a quadratic fit for the third quartile yields essentially the same result as the linear fit; in other words, the coefficient of the L^2 term using a quadratic fit is nearly zero.)

[34] A linear fit for the mean value of the base 10 logarithm of $dn_{e,eq}/dt$ (thick solid red curve in Figures 9a and 9b) yields

$$\frac{dn_{e,eq}}{dt} = 10^{2.74-0.269L}\left(\mathrm{cm}^{-3}/\mathrm{day}\right), \tag{11}$$

and this is plotted as the thick dotted red curve in Figure 9b.

3.3. Solar Cycle Dependence

[35] Now we examine the solar cycle dependence of the refilling rate $dn_{e,eq}/dt$. We break our set of quiet time events into two groups. The first group extends from the 33rd day of 2001 to the 265th day of 2002, and corresponds most closely to solar maximum. The second group extends from the 352nd day of 2003 to the 356th day of 2005, and corresponds most closely to solar minimum. (There were no quiet time events between these two intervals.) The two time intervals are indicated in Figure 12 by the horizontal lines labeled "max" for the interval corresponding to solar maximum and "min" for the interval corresponding to solar minimum. Note that while our "min" period has significantly less

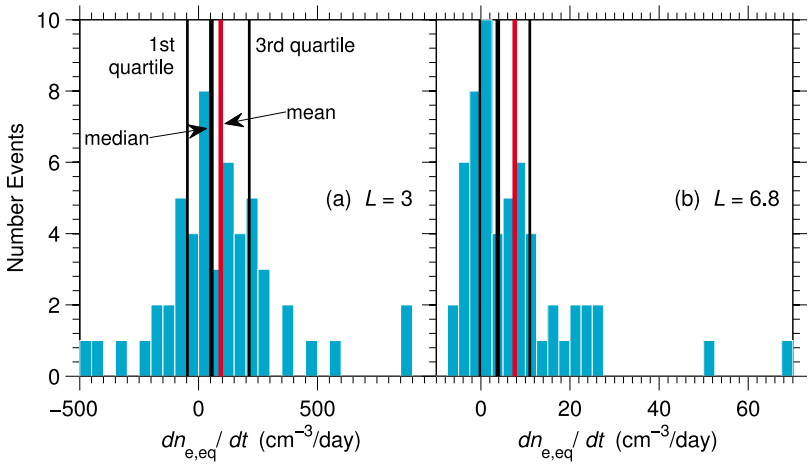

Figure 7. Histogram of refilling rates $dn_{e,eq}/dt$ at (a) $L = 3$ and (b) $L = 6.8$. The left thin solid black vertical line, black thick solid vertical line, right black thin solid vertical line, and red thick solid vertical line are drawn at a horizontal position corresponding to the first quartile, median, third quartile, and mean values, respectively.

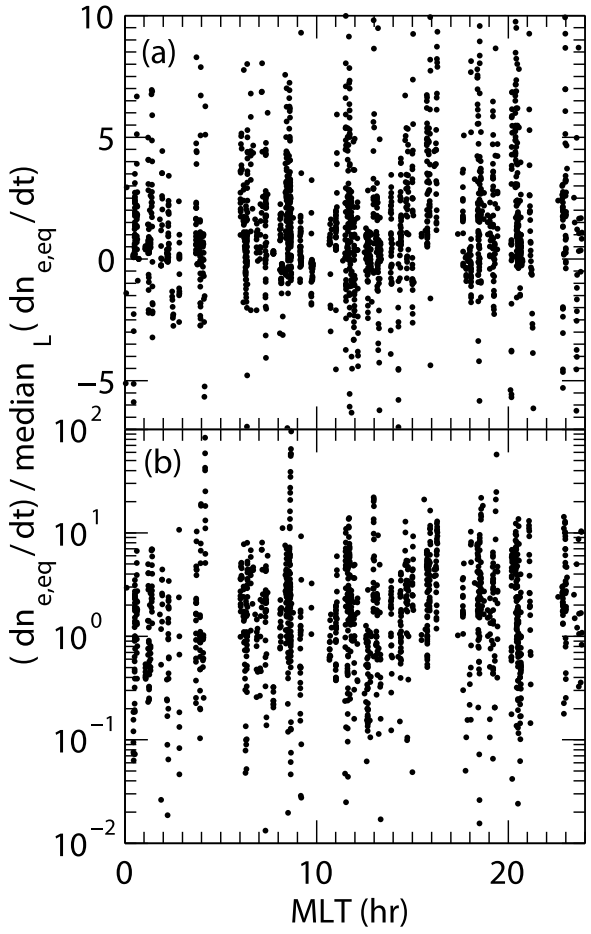

Figure 8. Individual refilling rates $dn_{e,eq}/dt$ normalized to the median rate for that particular L shell for a set of L shells varying between 2 and 9 and plotted versus MLT on a (a) linear scale and (b) log scale.

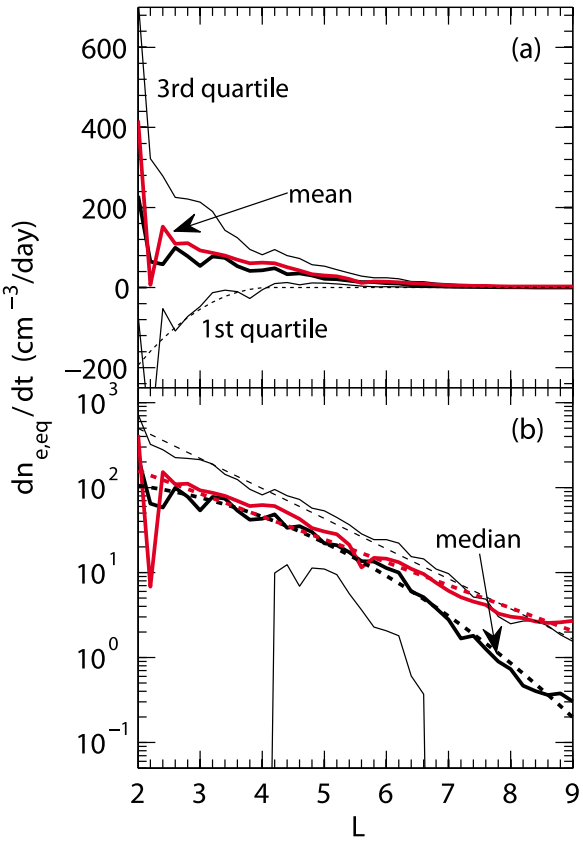

Figure 9. Values of the refilling rate $dn_{e,eq}/dt$ (in cm^{-3}) versus L plotted using (a) linear and (b) log scales. The lower thin solid, thick solid, and upper thin solid black curves are respectively the first quartile, median, and third quartile values; the red curve is the mean value. The dotted curves are fits as described in the text.

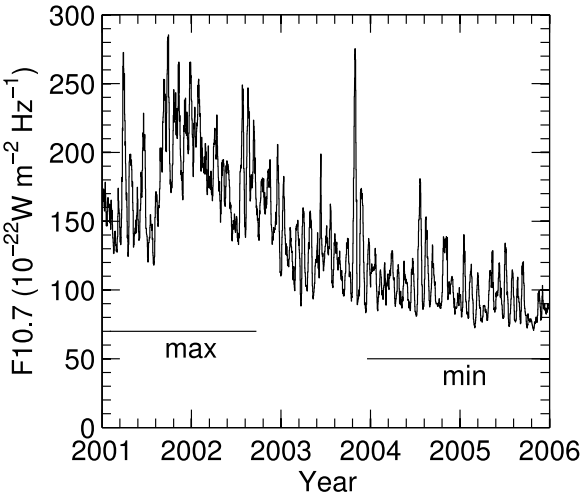

Figure 10. Plot of F10.7 solar EUV index versus time in years with the line labeled "max" indicating the interval corresponding most closely to solar maximum, and the line labeled "min" indicating the interval most closely corresponding to solar minimum.

solar EUV radiation, it is not the real solar minimum which occurred later, and the F10.7 values that occurred during that time (Figure 12) are not as low as those that sometimes occur at solar minimum ($<80 \times 10^{-22}$ Wm^{-2} Hz^{-1}). Nevertheless, this period will serve to illustrate the difference in refilling rate during the solar cycle.

[36] Again we calculate the median and third quartile refilling rates $dn_{e,eq}/dt$ and calculate fits. (We won't show results here for the first quartile which is typically negative or close to zero.) The results are shown in Figure 11. The median and third quartile refilling rates are larger at solar maximum for small $L < 4$, about the same at solar maximum and solar minimum for $L = 4.2$ to 5.8, and larger at solar minimum for large $L > 5.8$ such as at geostationary orbit ($L = 6.8$). The rates become comparable at large L (>8.5 and 8 for the third quartile and median, respectively), but the rates may be less reliable at this distance.

[37] A quadratic fit for the base 10 logarithm of the median $dn_{e,eq}/dt$ value is

$$\log_{10}\left(\frac{dn_{e,eq}}{dt}\right) = 2.76 - 0.153L - 0.0277L^2, \quad \text{at solar max,} \quad (12)$$

$$= 1.01 + 0.419L - 0.0679L^2, \quad \text{at solar min,} \quad (13)$$

where $dn_{e,eq}/dt$ is expressed in cm^{-3}/day here and in subsequent equations. (One negative value for the median of $dn_{e,eq}/dt$ at $L = 2.5$ for solar minimum (note the gap in the thick blue curve in Figure 11) was ignored for the fit. Note that there is a data point at $L = 2$.) A linear fit for the base 10 logarithm of the third quartile $dn_{e,eq}/dt$ value is

$$\log_{10}\left(\frac{dn_{e,eq}}{dt}\right) = 3.54 - 0.379L, \quad \text{at solar max,} \quad (14)$$

$$= 3.26 - 0.331L, \quad \text{at solar min.} \quad (15)$$

A linear fit for the base 10 logarithm of the mean $dn_{e,eq}/dt$ value is

$$\log_{10}\left(\frac{dn_{e,eq}}{dt}\right) = 3.01 - 0.322L, \quad \text{at solar max,} \quad (16)$$

$$= 2.87 - 0.282L, \quad \text{at solar min.} \quad (17)$$

(Again one negative value for the median of $dn_{e,eq}/dt$ at $L = 2.5$ for solar minimum was ignored for the fit.)

4. Discussion

4.1. Other Types of Refilling

[38] *Su et al.* [2001] found that the short term (<1 day, or diurnal) refilling rate increased with increasing geomagnetic activity. In principle, we ought to be able to investigate the long-term refilling rate for greater geomagnetic activity also, at least for low values of L for which corotation still dominates. We looked for time periods of 1.5 day or greater with Kp between 1.5 and 3 and with the daily average of Kp for the preceding day greater than 2.5. This last condition is required so that we make sure that we are not looking at a period of erosion due to magnetospheric convection following a more quiet time period. But there were simply too few events of this type to be statistically useful for our method.

[39] It may also be possible to investigate short-term refilling using the IMAGE data. A model could be chosen for the MLT dependence using a small number of parameters (like several Fourier coefficients), and the model parameters could be adjusted so as to minimize the error in the predicted steps in $n_{e,eq}$ from one pass of the spacecraft through a region with a particular MLT value to the next pass through that region. But we leave this for another study.

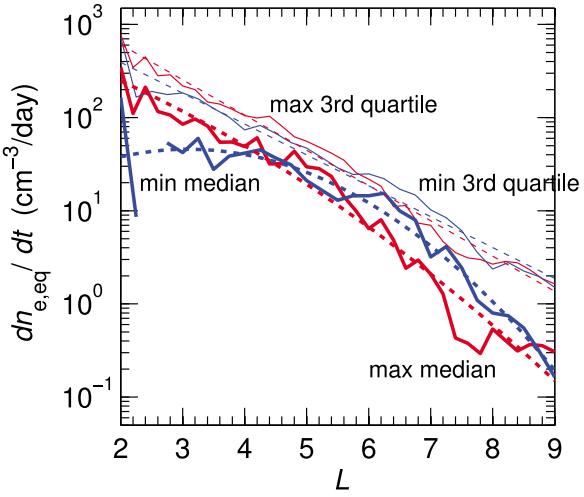

Figure 11. Median (thick solid curves) and third quartile (thin solid curves) for the refilling rate $dn_{e,eq}/dt$ during intervals corresponding to solar maximum (red curves) and solar minimum (blue curves). The dotted curves are the corresponding quadratic fits described in the text.

4.2. Saturation

[40] While not all studies of refilling have found that the density saturates (reaches a maximum value) [*Park*, 1970; *Krall et al.*, 2008], some clearly did observe that refilling stops when the density saturates at a high value [*Park*, 1974; *Sojka and Wrenn*, 1985; *Lawrence et al.*, 1999; *Chi et al.*, 2000; *Su et al.*, 2001]. So the question naturally arises, "why do we not see such saturation in our data set?" The answer seems to be that saturation only occurs after a long period of refilling during quiet conditions, and none of our events fits this criterion. *Su et al.* [2001] had 20 events with 6 days of refilling, whereas we only have 4 events with more than 4 days of refilling, and none with 5 days of refilling. Presumably if the lifetime of the IMAGE spacecraft had lasted beyond the beginning of 2006 extending into the very quiet solar minimum of this last solar cycle, we would have had many more long quiet intervals, but we do not have these in our data set. Another way of looking at it is to consider the saturation density. Su et al. found that this was 100–200 cm^{-3} at geostationary orbit. But Figure 4 shows that $n_{e,eq}$ at geostationary orbit does not reach 100 cm^{-3} during our quiet time events. Therefore it appears that while it may be possible for the density to saturate, this is a relatively unlikely occurrence, especially at times other than solar minimum.

4.3. Comparison to Previous Results

[41] Figure 1 shows our median, quartile, and mean refilling rates $dn_{e,eq}/dt$ along with results from previous studies. Clearly many of the refilling rates found in previous studies shown in Figure 1 are larger than those typically found in our study. But as we pointed out in the Introduction, most of these previous studies used a single event, and it may be that the authors of some of these studies picked out events that dramatically exhibited strong refilling. As shown in subsection 3.1, refilling rates may vary greatly depending on the event chosen. Our purpose is to calculate and model typical rates of refilling.

[42] The best statistics of any previous study are presented by *Su et al.* [2001]. Their results are presented in Figure 1 at $L = 6.8$ as "Su", with bold, normal, and italic face for solar maximum, rising or falling phase of the solar cycle, or solar minimum, respectively. Near these symbols in Figure 1, we draw vertical lines from the median to third quartile refilling rates from our study for our periods of solar maximum and solar minimum. That is, the bottom of each of these vertical lines is plotted at the median value while the top of each of these vertical lines is plotted at the third quartile value. These are offset slightly to the left and right of the "Su" symbols in order to be able to see all of these objects clearly, but the vertical lines should be considered properly to be horizontally centered on the "Su" symbols. It appears then that the Su et al. refilling rates $dn_{e,eq}/dt$ for both solar maximum and solar minimum are between our median and third quartile rates, but closer to the third quartile rates.

[43] As is clear from Figure 9 (and Figure 1), our mean refilling rates are close to the median values at small $L < 6$, but are larger than the median values for $L > 6$, and are roughly equal to the quartile values at $L = 8.5$. It's a little bit difficult to directly compare the method of Su et al. with ours; they use a linear fit to 70th percentile values of density in bins of time from the start of the quiet event. But it is possible that their values correspond more directly with our mean values.

[44] The fact that our mean refilling rates are close to the median values for low $L = 3$ but in between the median and third quartile values for $L = 6.8$ can also be seen from the histograms in Figure 7. At $L = 3$, the distribution of refilling times is more Gaussian than that at $L = 6.8$. At $L = 3$, the possible negative refilling rates are of comparable size to the possible positive refilling rates. At $L = 6.8$, however, there is a tail extending to large positive values in the distribution of refilling rates. This distribution is more like a Poisson distribution that could occur if refilling rates are limited to values above zero.

[45] We also found the 90 percentile values with our data set (not shown). These rates are roughly a factor of two above the third quartile rates in Figure 1. The maximum rates found in our study are plotted as dots in Figure 1. Most of the results shown in Figure 1 would lie under our 90 percentile rates, and all of them lie under the maximum rates except that of *Sandel and Denton* [2007] ("Sl" symbol in Figure 1) at $L = 5$. This event could represent extraordinarily rapid refilling. On the other hand, to calculate the refilling rate for $n_{e,eq}$ based on results of Sandel and Denton, we had to assume a model for the n_{He+}/n_{H+} ratio that might not be valid for this particular event.

4.4. Solar Cycle Dependence

[46] Figure 11 shows our refilling rates broken down into periods that most closely correspond to solar maximum (red curves) and solar minimum (blue curves). Based on our data, the refilling rate is larger at geostationary orbit ($L = 6.8$) for solar minimum (blue curves), and the difference in our rates for these two periods is roughly consistent with the previous study of *Su et al.* [2001] (Figure 1). But Figure 11 indicates that at smaller L values ($L = 4.2$ to 5.8), the refilling rates for the two periods become comparable, and that at even smaller L values ($L < 4$), the refilling rate at solar maximum becomes larger than the refilling rate at solar minimum. This seems to be consistent with most of the results of previous studies at low L, which can be seen from examination of Figure 1 for $L \leq 4$. (The bold symbols are generally higher on the plot.) The exception seems to be the refilling rate of *Chi et al.* [2000] ("Ci" symbol in Figure 1), which is very high though not at solar maximum. But as already pointed out in the Introduction, Chi et al. directly measure mass density, not electron density, and there is some evidence that the average ion mass becomes greater than 1 amu at $L < 3$ [*Dent et al.*, 2006].

[47] While ionospheric electron density is typically higher at solar maximum for all L, the solar cycle dependence of H+ is more complicated, and therefore the solar cycle dependence of electron density at the magnetic equator (where H+ ions are dominant) may also be more complicated. In fact, previous results at geostationary orbit indicate that while the O+ concentration is typically higher at solar maximum, the electron density is typically higher at solar minimum [*Denton et al.*, 2011].

[48] In order to investigate the cause of our different solar cycle dependence at different L values, we examined the solar cycle dependence of ionospheric density. Figure 12a shows values of n_e versus L (calculated from geomagnetic

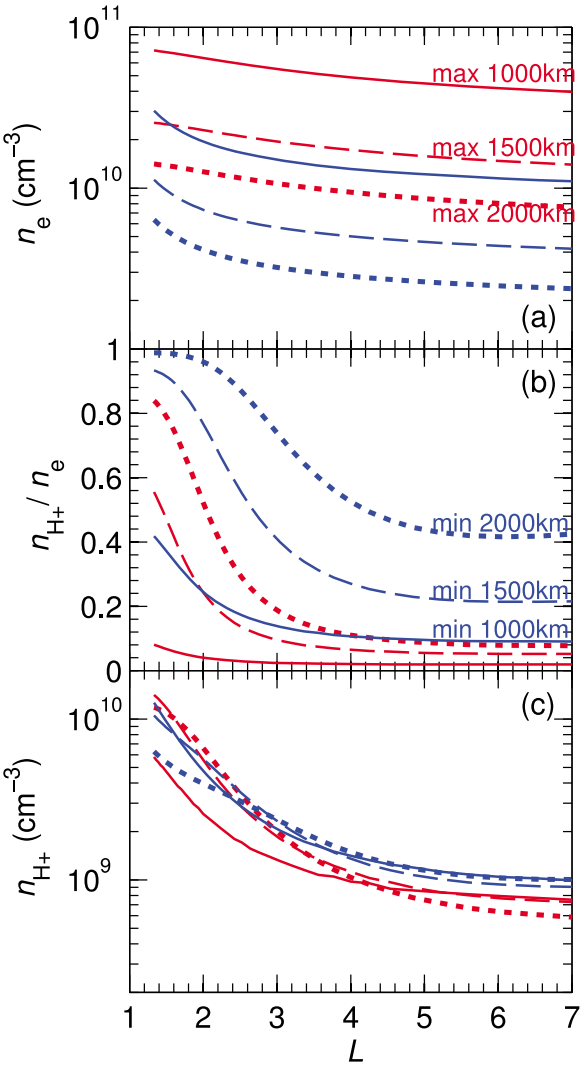

Figure 12. International Reference Ionosphere (IRI) 2007 model values of (a) n_e, (b) n_{H+}/n_e, and (c) n_{H+} versus L. The red curves are at solar maximum, while the blue curves are at solar minimum, and the solid, dashed, and dotted curves are at 1000 km, 1500 km, and 2000 km, respectively.

latitude assuming a dipole magnetic field) at noon local time at the spring equinox (21 Sept) from the International Reference Ionosphere (IRI) 2007 model [*Bilitza and Reinisch*, 2008]. The red curves are calculated for year 2002, and correspond most closely to solar maximum, while the blue curves are calculated for year 2005, and correspond most closely to solar minimum. (These times are also fairly central to our time periods for solar maximum and solar minimum shown in Figure 10.) The solid curves are at 1000 km, while the dashed curves are at 1500 km, the highest height at which the IRI model is considered to be accurate (D. Bilitza, private communication, 2011). The dotted curves are the values extrapolated to 2000 km (which are also found from the IRI). Note that the electron density decreases uniformly with respect to altitude for any L and is also lower at solar minimum (blue curves) than at solar maximum (red curves) at any height and at any L. The concentration of H+, n_{H+}/n_e, is shown in Figure 12b. This quantity has exactly the opposite dependencies to those of n_e. The value of n_{H+}/n_e increases with respect to height (moving from solid to dashed to dotted curves) and from solar maximum to solar minimum (moving from red curves to blue curves).

[49] The H+ density n_{H+} is the product of n_e and n_{H+}/n_e. This quantity is plotted in Figure 12c, and there is not nearly as great a variation of n_{H+} with respect to height and phase of the solar cycle. Nevertheless, there is a very interesting difference in the solar cycle dependence with respect to L. At 1000 km, the H+ density is higher at solar minimum (solid blue curve) then at solar maximum (solid red curve) for any L. Apparently the n_{H+}/n_e solar cycle dependence is stronger than that of n_e. But at 1500 km (dashed curves), for $L < 2$, the H+ density is greater at solar maximum (dashed red curve) than at solar minimum (dashed blue curve), while for $L > 2$, the H+ density is greater at solar minimum (dashed blue curve) than at solar maximum (dashed red curve). Furthermore, the extrapolated densities at 2000 km show that the borderline L value moves outward. At 2000 km (dotted curves), for $L < 2.7$, the H+ density is greater at solar maximum (dotted red curve) than at solar minimum (dotted blue curve), while for $L > 2.7$, the H+ density is greater at solar minimum (dotted blue curve) than at solar maximum (dotted red curve).

[50] Note that the general trend in Figure 12 seems to be for the H+ density to be higher at solar minimum than at solar maximum (blue curves above the red curves for most L values in Figure 12c) because of the greater concentration of H+ at solar minimum (Figure 12b). But at low L values, there is a large change in the H+ concentration with respect to altitude only for solar maximum. At these low L values, the plasma is almost totally H+ even at 1500 km (dashed blue curve in Figure 12b). As we move farther up to 2000 km (dotted blue curve in Figure 12b), there is at these low L values little change in the H+ concentration, and the drop in electron density with respect to altitude (Figure 12a) leads to a consequent drop in the H+ density (dotted blue curve lower than solid and dashed blue curves in Figure 12c).

[51] These observations also appear to be roughly consistent with spacecraft observations of ion composition published by *Truhlik et al.* [2005]. First of all, their data confirms the idea that there might be lower hydrogen density at solar maximum. There is an issue about the range of L. Truhlik et al.'s data is for very low L. Zero degrees invariant latitude in their paper corresponds to $L \sim 1$ based on the dipole field mode and 50° invariant latitude corresponds roughly to $L = 2.5$. We found that the H+ density is higher at solar minimum than at solar maximum for all L at 1000 km altitude (comparing the solid red and blue curves in Figure 12c), for $L > 2$ at 1500 km altitude (comparing the dashed red and blue curves in Figure 12c), and for $L > 2.6$ at 2000 km altitude (comparing the dotted red and blue curves in Figure 12c). So our data would suggest that at the low L values studied by Truhlik et al., the H+ density should decrease with respect to solar activity at low altitudes (1000 km or less), but increase with respect to solar activity at high altitudes (by at least 2000 km). In fact, Truhlik et al.'s data show that the H+ density decreases with respect to F10.7 at 600 km (bottom left panels of *Truhlik et al.*'s [2005] Figures 3 and 4), that the trend with respect to F10.7 becomes somewhat weaker at 850 km (bottom left panels of *Truhlik et al.*'s [2005] Figures 5 and 6; note that the range of

decrease in density is now smaller), and that the trend disappears at an altitude of 1300 km (bottom left panel of *Truhlik et al.*'s [2005] Figure 9). If the trend we are seeing in Truhlik et al.'s data continues to higher altitude, it may reverse so that the hydrogen density becomes greater for larger F10.7 at even higher altitude like 1500 or 2000 km.

[52] At geostationary orbit, the dominant contribution to the electron density is from H+ (though the mass density may be dominated by O+ at solar maximum) [*Denton et al.*, 2011]. Therefore, if the electron density refilling rate varies roughly like the H+ density, at the magnetic equator (very high altitude), we might expect the refilling rate to be greater at solar maximum at low L and greater at solar minimum at high L with a borderline value of L greater than 2.7 based on the dependencies we see in the ionosphere; and this is what we observed in Figure 12, where the borderline L value was between 4.2 and 5.8.

5. Summary

[53] We have used measurements of the electron density n_e found from passive radio wave observations by the IMAGE RPI instrument along with a model for the field line dependence (7) to estimate the equatorial electron density $n_{e,eq}$, and then have used these values on two or more passes through a particular region of local time in order to evaluate the linear long-term (>1 day) refilling rate. Lower refilling rate for the first day of refilling, as has been observed by some other researchers [*Lawrence et al.*, 1999; *Su et al.*, 2001; *Dent et al.*, 2006] was not clearly observed in our data; and saturation [*Park*, 1974; *Sojka and Wrenn*, 1985; *Lawrence et al.*, 1999; *Chi et al.*, 2000; *Su et al.*, 2001] was also not observed, perhaps because we did not have long enough periods of quiet in order to reach saturation, as was discussed in section 4.2. Because of these facts, we found it adequate to characterize our refilling rates by a single linear value $dn_{e,eq}/dt$. Then at each L value, we found the first quartile, median, third quartile, and mean values of $dn_{e,eq}/dt$. While statistical results for refilling have been made at geostationary orbit (especially *Lawrence et al.* [1999] and *Su et al.* [2001]), this is the first statistical study of refilling over a large range of L shell, 2–9.

[54] Our results are plotted in Figure 9, and can be modeled as (9) repeated here

$$\frac{dn_{e,eq}}{dt} = 10^{2.22-0.006L-0.0347L^2}\left(\mathrm{cm}^{-3}/\mathrm{day}\right) \tag{18}$$

for the median refilling rate in cm^{-3}/day, and (10) repeated here

$$\frac{dn_{e,eq}}{dt} = 10^{3.39-0.353L}\left(\mathrm{cm}^{-3}/\mathrm{day}\right) \tag{19}$$

for the third quartile refilling rate, and (11) repeated here

$$\frac{dn_{e,eq}}{dt} = 10^{2.74-0.269L}\left(\mathrm{cm}^{-3}/\mathrm{day}\right) \tag{20}$$

for the mean rate. (The first quartile rates are usually negative, and can be roughly modeled by (8).) The mean values are close to the median values for $L < 6$, but are closer to the third quartile values at geostationary orbit (L = 6.8) and beyond. Our third quartile refilling rate seems to be more characteristic of most previous studies than the median refilling rate, as can be seen from Figure 1. Dividing the typical plasmasphere density (3) by these rates (as was done in the Introduction), we can estimate characteristic refilling times, and we plot these in Figure 2. Our refilling times are larger than the bulk of those discussed in the Introduction. As we showed in section 4.3, our results are roughly consistent with those of *Su et al.* [2001] at geostationary orbit (especially considering the difference in method). Many of the results listed in the Introduction apparently represent unusually strong refilling.

[55] We also examined the solar cycle dependence of the refilling rate $dn_{e,eq}/dt$ and the results are presented in Figure 11. Comparing refilling rates at solar maximum to those at solar minimum, we found that the median refilling rate is larger at solar maximum for small $L < 4.2$, about the same at solar maximum and solar minimum for L = 4.2 to 5.8, and is larger at solar minimum for large $L > 5.8$ such as at geostationary orbit (L = 6.8). This result seem to be roughly consistent with that of previous studies, and is also roughly consistent with trends for density from the IRI model and spacecraft observations by *Truhlik et al.* [2005], as discussed in section 4.4.

[56] **Acknowledgments.** This research was supported by NSF grant ATM-0751002. Work at Dartmouth College was further supported by NASA grants NNX10AQ60G (Living with a Star Targeted Research Plasmasphere focused science topic) and NNX11AO59G (Heliophysics Theory Program). We acknowledge useful conversations with Dieter Blitza, Vladimir Truhlik, and Stan Solomon.

[57] Masaki Fujimoto thanks the reviewers for their assistance in evaluating this paper.

References

Benson, R. F., P. A. Webb, J. L. Green, L. Garcia, and B. W. Reinisch (2004), Magnetospheric electron densities inferred from upper-hybrid band emissions, *Geophys. Res. Lett.*, *31*, L20803, doi:10.1029/2004GL020847.

Bilitza, D., and B. W. Reinisch (2008), International Reference Ionosphere 2007: Improvements and new parameters, *Adv. Space Res.*, *42*(4), 599–609, doi:10.1016/j.asr.2007.07.048.

Carpenter, D. L., and R. R. Anderson (1992), An ISEE/Whistler model of equatorial electron-density in the magnetosphere, *J. Geophys. Res.*, *97*(A2), 1097–1108.

Carpenter, D. L., B. L. Giles, C. R. Chappell, P. M. E. Decreau, R. R. Anderson, A. M. Persoon, A. J. Smith, Y. Corcuff, and P. Canu (1993), Plasmasphere dynamics in the duskside bulge region: A new look at an old topic, *J. Geophys. Res.*, *98*(A11), 19,243–19,271.

Chappell, C. R. (1974), Detached plasma regions in magnetosphere, *J. Geophys. Res.*, *79*(13), 1861–1870, doi:10.1029/JA079i013p01861.

Chen, S. H., and T. E. Moore (2006), Magnetospheric convection and thermal ions in the dayside outer magnetosphere, *J. Geophys. Res.*, *111*, A03215, doi:10.1029/2005JA011084.

Chi, P. J., C. T. Russell, S. Musman, W. K. Peterson, G. Le, V. Angelopoulos, G. D. Reeves, M. B. Moldwin, and F. K. Chun (2000), Plasmaspheric depletion and refilling associated with the September 25, 1998 magnetic storm observed by ground magnetometers at L = 2, *Geophys. Res. Lett.*, *27*(5), 633–636.

Craven, P. D., D. L. Gallagher, and R. H. Comfort (1997), Relative concentration of He+ in the inner magnetosphere as observed by the DE 1 retarding ion mass spectrometer, *J. Geophys. Res.*, *102*(A2), 2279–2289.

Darrouzet, F., J. De Keyser, P. M. E. Decreau, F. El Lemdani-Mazouz, and X. Vallieres (2008), Statistical analysis of plasmaspheric plumes with Cluster/WHISPER observations, *Ann. Geophys.*, *26*(8), 2403–2417.

Dent, Z. C., I. R. Mann, J. Goldstein, F. W. Menk, and L. G. Ozeke (2006), Plasmaspheric depletion, refilling, and plasmapause dynamics: A coordinated ground-based and IMAGE satellite study, *J. Geophys. Res.*, *111*, A03205, doi:10.1029/2005JA011046.

Denton, R. E. (2006), Magneto-seismology using spacecraft observations, in *Magnetospheric ULF Waves: Synthesis and New Directions*, *Geophys.*

Monogr. Ser., vol. 169, edited by K. Takahashi et al., pp. 307–317, AGU, Washington, D. C.

Denton, R. E., J. Goldstein, and J. D. Menietti (2002), Field line dependence of magnetospheric electron density, *Geophys. Res. Lett.*, *29*(24), 2205, doi:10.1029/2002GL015963.

Denton, R. E., J. D. Menietti, J. Goldstein, S. L. Young, and R. R. Anderson (2004), Electron density in the magnetosphere, *J. Geophys. Res.*, *109*, A09215, doi:10.1029/2003JA010245.

Denton, R. E., K. Takahashi, I. A. Galkin, P. A. Nsumei, X. Huang, B. W. Reinisch, R. R. Anderson, M. K. Sleeper, and W. J. Hughes (2006), Distribution of density along magnetospheric field lines, *J. Geophys. Res.*, *111*, A04213, doi:10.1029/2005JA011414.

Denton, R. E., M. F. Thomsen, K. Takahashi, R. R. Anderson, and H. J. Singer (2011), Solar cycle dependence of bulk ion composition at geosynchronous orbit, *J. Geophys. Res.*, *116*, A03212, doi:10.1029/2010JA016027.

Farrugia, C. J., D. T. Young, J. Geiss, and H. Balsiger (1989), The composition, temperature, and density structure of cold ions in the quiet terrestrial plasmasphere: GEOS 1 results, *J. Geophys. Res.*, *94*(A9), 11,865–11,891.

Fu, H. S., J. Tu, J. B. Cao, P. Song, B. W. Reinisch, D. L. Gallagher, and B. Yang (2010), IMAGE and DMSP observations of a density trough inside the plasmasphere, *J. Geophys. Res.*, *115*, A07227, doi:10.1029/2009JA015104.

Goldstein, J., and B. R. Sandel (2005), The global pattern of evolution of plasmaspheric drainage plumes, in *Inner Magnetosphere Interactions: New Perspectives From Imaging*, *Geophys. Monogr. Ser.*, vol. 159, edited by J. L. Burch, M. Schulz, and H. Spence, pp. 1–22, AGU, Washington, D. C.

Goldstein, J., B. R. Sandel, W. T. Forrester, and P. H. Reiff (2003), IMF-driven plasmasphere erosion of 10 July 2000, *Geophys. Res. Lett.*, *30*(3), 1146, doi:10.1029/2002GL016478.

Grebowsky, J. (1970), Model study of a plasmapause motion, *J. Geophys. Res.*, *75*(22), 4329–4333, doi:10.1029/JA075i022p04329.

Helliwell, R. A. (1965), *Whistlers and Related Ionospheric Phenomenon*, Dover, Mineola, New York.

Krall, J., J. D. Huba, and J. A. Fedder (2008), Simulation of field-aligned H+ and He+ dynamics during late-stage plasmasphere refilling, *Ann. Geophys.*, *26*(6), 1507–1516.

Lawrence, D. J., M. F. Thomsen, J. E. Borovsky, and D. J. McComas (1999), Measurements of early and late time plasmasphere refilling as observed from geosynchronous orbit, *J. Geophys. Res.*, *104*(A7), 14,691–14,704.

Lemaire, J., and K. Gringauz (1998), *The Earth's Plasmasphere*, Cambridge Univ. Press, New York.

Obana, Y., F. W. Menk, and I. Yoshikawa (2010), Plasma refilling rates for L = 2.3–3.8 flux tubes, *J. Geophys. Res.*, *115*, A03204, doi:10.1029/2009JA014191.

Park, C. G. (1970), Whistler on observations of interchange of ionization between ionosphere protonosphere, *J. Geophys. Res.*, *75*(22), 4249–4260, doi:10.1029/JA075i022p04249.

Park, C. G. (1974), Some features of plasma distribution in plasmasphere deduced from Antarctic whistlers, *J. Geophys. Res.*, *79*(1), 169–173, doi:10.1029/JA079i001p00169.

Persoon, A. M., D. A. Gurnett, and S. D. Shawhan (1983), Polar cap electron densities from DE-1 plasma wave observations, *J. Geophys. Res.*, *88*(A12), 10,123–10,136, doi:10.1029/JA088iA12p10123.

Reinisch, B. W., et al. (2001), First results from the Radio Plasma Imager on IMAGE, *Geophys. Res. Lett.*, *28*(6), 1167–1170, doi:10.1029/2000GL012398.

Reinisch, B. W., X. Huang, P. Song, J. L. Green, S. F. Fung, V. M. Vasyliunas, D. L. Gallagher, and B. R. Sandel (2004), Plasmaspheric mass loss and refilling as a result of a magnetic storm, *J. Geophys. Res.*, *109*, A01202, doi:10.1029/2003JA009948.

Sandel, B. R., and M. H. Denton (2007), Global view of refilling of the plasmasphere, *Geophys. Res. Lett.*, *34*, L17102, doi:10.1029/2007GL030669.

Singh, N., and J. L. Horwitz (1992), Plasmasphere refilling: Recent observations and modeling, *J. Geophys. Res.*, *97*(A2), 1049–1079, doi:10.1029/91JA02602.

Sojka, J. J., and G. L. Wrenn (1985), Refilling of geosynchronous flux tubes as observed at the equator by GEOS 2, *J. Geophys. Res.*, *90*(A7), 6379–6385.

Song, X. T., R. Gendrin, and G. Caudal (1988), Refilling process in the plasmasphere and its relation to magnetic activity, *J. Atmos. Terr. Phys.*, *50*(3), 185–195.

Su, Y. J., M. F. Thomsen, J. E. Borovsky, and D. J. Lawrence (2001), A comprehensive survey of plasmasphere refilling at geosynchronous orbit, *J. Geophys. Res.*, *106*(A11), 25,615–25,629, doi:10.1029/2000JA000441.

Takahashi, K., R. E. Denton, R. R. Anderson, and W. J. Hughes (2006), Mass density inferred from toroidal wave frequencies and its comparison to electron density, *J. Geophys. Res.*, *111*, A01201, doi:10.1029/2005JA011286.

Takahashi, K., S. Ohtani, R. E. Denton, W. J. Hughes, and R. R. Anderson (2008), Ion composition in the plasma trough and plasma plume derived from a Combined Release and Radiation Effects Satellite magnetoseismic study, *J. Geophys. Res.*, *113*, A12203, doi:10.1029/2008JA013248.

Truhlik, V., L. Triskova, and J. Smilauer (2005), Manifestation of solar activity in the global topside ion composition–A study based on satellite data, *Ann. Geophys.*, *23*(7), 2511–2517.

Tsyganenko, N. A. (1996), Effects of the solar wind conditions on the global magnetospheric configuration as deduced from data-based field models, in *European Space Agency Publication*, *Eur. Space Agency Spec. Publ.*, *ESA SP-389*, 181–185.

Tsyganenko, N. A., and M. I. Sitnov (2005), Modeling the dynamics of the inner magnetosphere during strong geomagnetic storms, *J. Geophys. Res.*, *110*, A03208, doi:10.1029/2004JA010798.

Webb, P., R. Benson, R. Denton, J. Goldstein, L. Garcia, and B. Reinisch (2007), An inner magnetospheric electron density database determined from IMAGE/RPI passive dynamic spectra, *Eos Trans. AGU*, *88*(52), Fall Meet. Suppl., Abstract SM12A-04.

R. E. Denton and P. M. Tengdin, Department of Physics and Astronomy, Dartmouth College, Hanover, NH 03755, USA. (richard.e.denton@dartmouth.edu; phoebe.tengdin@gmail.com)

J. Goldstein and J. A. Redfern, Southwest Research Institute, 6220 Culebra Rd., San Antonio, TX 78238, USA. (jgoldstein@swri.edu; jredfern@swri.edu)

B. W. Reinisch, Center for Atmospheric Research, University of Massachusetts at Lowell, 600 Suffolk St., Lowell, MA 01854, USA. (bodo_reinisch@uml.edu)

Y. Wang, NASA Goddard Space Flight Center, Code 674, Greenbelt, MD 20771, USA. (yongli.wang@nasa.gov)

P. A. Webb, Goddard Earth Sciences and Technology Center, University of Maryland, Baltimore County, 5523 Research Park Dr., Ste. 320, Baltimore, MD 21228, USA. (spacesheep@gmail.com)